Self-Powered Pulse Sensor for Antidiastole of Cardiovascular Disease

Han Ouyang, Jingjing Tian, Guanglong Sun, Yang Zou, Zhuo Liu, Hu Li, Luming Zhao, Bojing Shi, Yubo Fan, Yifan Fan, Zhong Lin Wang,* and Zhou Li**

Cardiovascular diseases are the leading cause of death globally; fortunately, 90% of cardiovascular diseases are preventable by long-term monitoring of physiological signals. Stable, ultralow power consumption, and high-sensitivity sensors are significant for miniaturized wearable physiological signal monitoring systems. Here, this study proposes a flexible self-powered ultrasensitive pulse sensor (SUPS) based on triboelectric active sensor with excellent output performance (1.52 V), high peak signal-noise ratio (45 dB), long-term performance (10^7 cycles), and low cost price. Attributed to the crucial features of acquiring easy-processed pulse waveform, which is consistent with second derivative of signal from conventional pulse sensor, SUPS can be integrated with a bluetooth chip to provide accurate, wireless, and real-time monitoring of pulse signals of cardiovascular system on a smart phone/PC. Antidiastole of coronary heart disease, atrial septal defect, and atrial fibrillation are made, and the arrhythmia (atrial fibrillation) is indicative diagnosed from health, by characteristic exponent analysis of pulse signals accessed from volunteer patients. This SUPS is expected to be applied in self-powered, wearable intelligent mobile diagnosis of cardiovascular disease in the future.

Cardiovascular diseases are one of the leading causes of death globally. It resulted in 17.3 million deaths (31.5%) in 2013 up from 12.3 million (25.8%) in 1990.[1] However, it is estimated that 90% of cardiovascular diseases are preventable.[2] The invention of various medical sensors[3] based on electrocardiograph (ECG),[4] phonocardiogram,[5] ambulatory blood pressure,[6] and sphygmograph[7] offers new opportunities in cardiovascular diseases prevention by the long-term monitoring of physiological signal. Pulse sensors have received extensive attention because of their noninvasive and convenient in usage. Nowadays, most widely used technologies for pulse measurement are photoplethysmography (PPG) and piezoelectric pulse transducer (PPT). However, the conventional pulse measurements of PPT and PPG are rarely employed directly, due to the difficulties in reading and analysis. After an operation of second derivative, the pulse measurements are often used to evaluate the heights of each wave and recognize the changes in the pulse waveforms for its simplicity.[8] Additionally, PPG is too sensitive and vulnerable to body movement and ambient light variation. Thus it is difficult to precisely measure pulse rates.[9] PPT is possibly limited by the low sensitivity and high cost. Furthermore, the energy consumption of the sensor is remained as a challenge for the miniaturization and weight reduction of mobile physiological signal monitoring system. Therefore, developing a self-powered, high-sensitivity, and low-cost pulse

H. Ouyang, J. J. Tian, Y. Zou, Z. Liu, H. Li, L. M. Zhao, Dr. B. J. Shi, Prof. Z. L. Wang, Prof. Z. Li
Beijing Institute of Nanoenergy and Nanosystems
Chinese Academy of Sciences
Beijing 100083, China
E-mail: zlwang@gatech.edu; zli@binn.cas.cn

H. Ouyang, J. J. Tian, Y. Zou, L. M. Zhao, Dr. B. J. Shi, Prof. Z. L. Wang, Prof. Z. Li
CAS Center for Excellence in Nanoscience
National Center for Nanoscience and Technology (NCNST)
Beijing 100190, China

H. Ouyang, J. J. Tian, Y. Zou, L. M. Zhao, Dr. B. J. Shi
University of Chinese Academy of Sciences
Beijing 100049, China

G. L. Sun
Department of Cardiac Surgery
Beijing Anzhen Hospital
Capital Medical University
Beijing Institute of Heart Lung and Blood Vessel Disease
Beijing 100029, China

Z. Liu, H. Li, Prof. Y. B. Fan
School of Biological Science and Medical Engineering
Beihang University
Beijing 100191, China

Prof. Y. F. Fan
Department of Cardiology
Beijing Chaoyang Hospital
Capital Medical University
Beijing Key Laboratory of Hypertension
Beijing 100020, China
E-mail: dryifan@163.com

Prof. Z. L. Wang
School of Materials Science and Engineering
Georgia Institute of Technology
Atlanta, GA 30332-0245, USA

The ORCID identification number(s) for the author(s) of this article can be found under https://doi.org/10.1002/adma.201703456.

DOI: 10.1002/adma.201703456

Table 1. The peak signal to noise ratio, electric output, power consumption, response time, and cost comparison between SUPS, PPT, and PPG.[13]

	Peak signal-to-noise ratio [dB]	Electric output [mV]	Power consumption [μW]	Response time [μs]	Cost price [$]
SUPS	45	1520	0	<50	0.2
PPT	26	12	0	<50	2
PPG	23	/	425	<1000	1

sensor which can directly acquire easy-processed pulse signal is urgent and significantly important.

Most recently, triboelectric nanogenerator (TENG) has been invented as a promising energy conversion approach for sustainable and continuous driving personal electronics.[10] It has been demonstrated that biomechanical energy could be harvested and converted into electric power through TENG.[11] Moreover, abundant physiological and biomedical information are contained in the electrical outputs of TENG, providing a self-powered active sensor for detecting biomechanical motion.[12]

Here, we propose a flexible, self-powered ultrasensitive pulse sensor (SUPS) based on triboelectric active sensor with excellent output performance, high peak signal-noise ratio (PSNR), ultrasensitive, and low cost (**Table 1**).[13] The SUPS can directly acquire voltage signal consistent with second derivative of conventional pulse signal without complex circuit design, mathematical operations, and the resulting error. A bluetooth chip enables wireless data transmission, and the pulse waveform is displayed on the intelligent terminals (smart phone or computer) in real time (Videos S1 and S2, Supporting Information). SUPS can provide accurate, wireless, and real-time monitoring of physiological information for cardiovascular diseases based on pulse signal. Through characteristic exponent analysis including heart rate variability (HRV) Poincare plot, time-domain HRV indexes, pulse contour analysis of these signals accessed from volunteer patients who have coronary heart disease (CHD), atrial septal defect (ASD), and atrial fibrillation (AF), SUPS provides indicative diagnosis and antidiastole to cardiovascular diseases. Pulse wave velocity (PWV) was also measured by simultaneously use two SUPSs, which can be used to indicate the degree of arteriosclerosis. This SUPS is expected to be applied in self-powered, wearable intelligent mobile diagnosis, and prevention of cardiovascular disease in the future.

The as-fabricated SUPS consists of two friction layers, electrode layers, and spacer, with all device structures were encapsulated inside by elastomer (**Figure 1**a). Nanostructured Kapton (n-Kapton) thin film (20 mm × 10 mm × 0.1 mm) as employed as one triboelectric layer. An ultrathin Cu layer (50 nm) was deposited on the back side of the Kapton film to form one of the electrodes. At the same time, an ultrathin Cu film (50 nm) was deposited on the previous n-Kapton film to obtain a nanostructured Cu (n-Cu) film (Figure S1a, Supporting Information) served both as the other triboelectric layer and electrode (Figure 1b,c). The entire device was packaged by a flexible polydimethylsiloxane (PDMS) layer (0.3 mm) to enhance its structural stability (Figure S1b, Supporting Information).[14]

The operating principle of the SUPS is based on the coupling of contact electrification and electrostatic induction. As shown in Figure 1d, when an external force is applied, two triboelectric layers were brought into contact with each other, and contact area that related to external forces were changed. Surface charge transfer then take place at the contact area due to triboelectrification effect. The electrons were transferred from the surface of n-Cu onto n-Kapton, resulting in net negative charges at the n-Kapton surface and net positive charges at the n-Cu surface, respectively. When the external force is released, in order to balance the electric potential difference established by the tribocharges on the n-Cu and n-Kapton films, the electrons in the attached Cu induction electrodes and n-Cu will be driven to flow back and forth through the external circuit, thus contributing to an electrical signal modulated by external force. The device with concave structures made contact electrification and electrostatic induction simultaneously, ensuring a good corresponding between external force and electrical signal of SUPS. Furthermore, a higher PSNR may attribute to the continuous contact of two friction layers, the artifact due to discontinuous contact was vanished. All of the above features and advantages lay a foundation to the further physiological and pulse signal detection.

The surface nanoarchitectures of two friction layers are important for the output performance of SUPS. A linear motor with the vertically compressive force about 50 N was employed to measure the electrical output of various friction layers, the flat Kapton, flat Cu, n-Kapton, and n-Cu were selected in pairs to compare the electrical output. As shown in **Figure 2**a, the output voltage, current, transferred charge of group n-Kapton and n-Cu were up to ≈109 V, 2.73 μA, and 7.6 nC, respectively. However, the group of flat Kapton and n-Cu, n-Kapton and flat Cu, flat Kapton and flat Cu, were decreased to 85 V, 1.71 μA, and 6.4 nC; 48 V, 0.84 μA, and 5.8 nC; 21 V, 0.39 μA, and 1.9 nC, respectively. Additionally, the real-time voltages, current, and transferred charge on radial arteries were recorded. When SUPS was pressed on the radial arteria of a 24 year old man, the voltage, current, transferred charges of the group of n-Kapton and n-Cu were 1.52 V, 5.4 nA, and 1.08 nC, significantly higher than other groups (Figure 2b). These differences may attribute to that the actual contact area of friction layers is further increased owing to the flexible nanostructures, and the charge transfer was promoted by the tip discharge effect of the nanoelectrode.

In order to present an intuitive view to the ultrasensitivity of SUPS, a honeybee with the low amplitude was employed to test (Figure 2c). The SUPS can reliably detect the mechanical vibration signals of honeybee wings and converted it into electrical signals. The output voltage was up to 0.5 V and the frequency is consistent with the vibration frequency of the honeybee wings[15] (Figure S2a,b, Supporting Information). In addition, SUPS can accurately detect 10 kHz mechanical

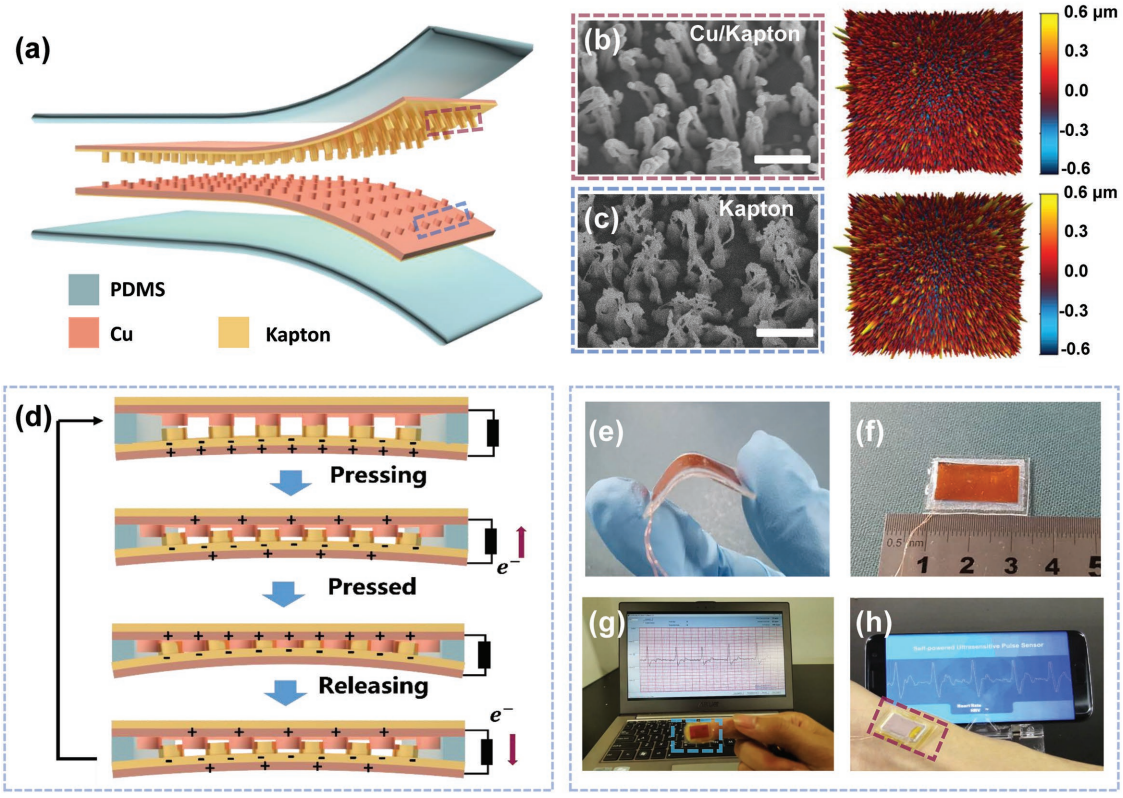

Figure 1. Structure, working principle, flexibility, and pulse signal output of SUPS. a) Schematic diagram of BD-TENG. b, c) SEM and atomic force microscopy (AFM) images of the nanostructure on the Cu and Kapton film, respectively (scale bar, 1 μm). d) Schematic diagram of the working principle of SUPS. e) Photograph of the bent SUPS demonstrating its good flexibility. f) Photograph of the size (2 cm × 1 cm) of SUPS. g, h) The real-time signal outputs when SUPS are placed over the finger and radial artery, respectively.

vibration signals from a small loudspeaker and converted it to electrical signals real-timely. The response time is as fast as 50 μs (Figure 2d). Generally, high-sensitive sensor was typically vulnerable to the overload external mechanical, so the long-term overload output performance and stability of SUPS were measured. Linear motor with a constant external mechanical force output of 30 N was used. The applied constant external mechanical force was more than 100 times of pulse pressure. As shown in Figure 2e; Figure S2c (Supporting Information), after one million working cycles, the open-circuit voltage of the SUPS was maintained stable at 20 V compared with its initial state, exhibiting its outstanding durability and stability. In addition, statistical analysis was also used to access the output voltage for 0.5 million cycles of triggering, and it showed no significant degradation ($P > 0.1055$; Figure S2d, Supporting Information).

Currently, the most persuasive pulse sensor used in clinical medicine was PPG. So to evaluate the reliability and match quality of SUPS in pulse wave monitoring, SUPS, PPT, (HK2000A) and PPG (TSD270B) were employed to compare with ECG (ECG100C). Traditionally, *R*–*R* interval of ECG is widely perceived as a sign of heartbeats, and was recognized as the reference standard for the accuracy and reliability of pulse sensor in tracking heart rate. As shown in **Figure 3**a, the peak waves of voltage output (SUPS, PPT, PPG) are synchronous to corresponding *R* waves in ECGs. Afterward, the linearity between *R*–*R* intervals measured by ECG (R–R_{ECG}) and peak intervals measured by the SUPS (P–P_{SUPS}), PPT (P–P_{PPT}), PPG (P–P_{PPG}) were detected, respectively. In Figure 3b–d, the data points (*R*–*R*n, *P*–*P*n) are shown as points while a linear fit is shown as a solid line. It showed a high linearity in R–R_{ECG} and P–P_{SUPS}, and the R^2 was 0.981 (Figure 3b), which was higher than values of 0.918 and 0.970 for PPT and PPG, respectively. These results demonstrated the accurate heart rate monitoring function of SUPS for heartbeats and revealed the potential of SUPS use in clinical medicine for pulse measurement.

The relationship and match quality between the signals of PPT, PPG, and SUPS were further detected using differential analysis techniques. As shown in Figure S3a in Supporting Information, the feature points (S, P, T, C, D) of PPT and its second derivative were strictly accordance with SUPS. And the R^2 was up to 0.9702 between SUPS and second derivative of PPT (Figure S3b,c, Supporting Information). Besides, the feature points (a–g) of SUPS were also consistent strictly with second derivative of PPG in timeline, there only have some differences in amplitude.[8,16] It may result from the differences in measurement location and principle (Figure S4a, Supporting Information). Since SUPS was attached on wrist and PPG was fixed on the finger (Figure S4b, Supporting Information) to acquire pulse signal.

In order to demonstrate the indicative diagnosis and antidiastole of SUPS to cardiovascular diseases, the pulse waveform

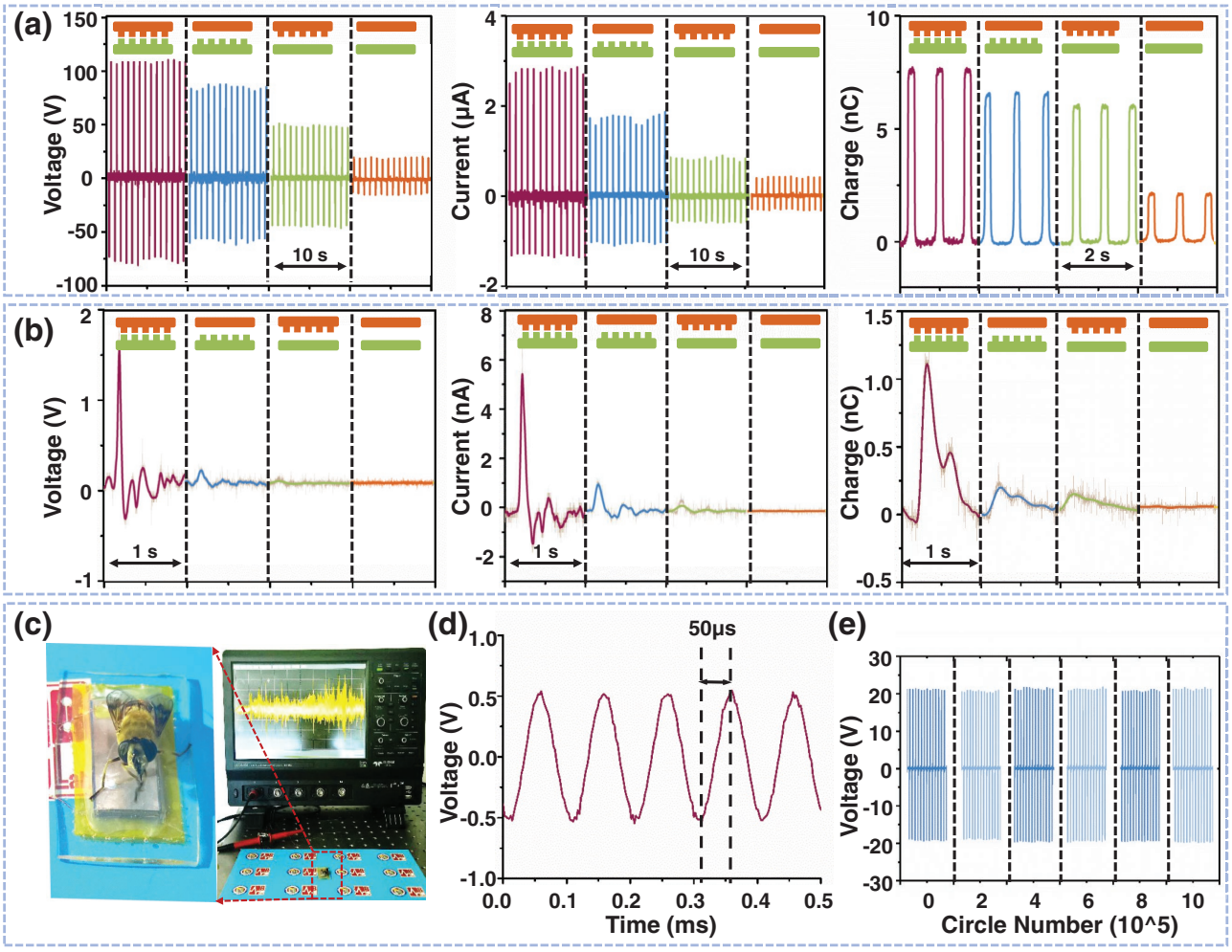

Figure 2. Electrical output modulating of SUPS by changing the surface structure of friction layers. a) The output voltage, current, and transferred charge of SUPS driven by a linear motor with different structure of friction layers. b) The output voltage, current, and transferred charge of SUPS pressed on the radial artery with different structure of friction layers. c) The optical image of bee wings on the SUPS, with the output performance driven by the bee wings (frequency, ≈200 Hz) display on the oscilloscope in real time. d) The output voltage of SUPS with the extremely high frequency of 10 KHz. e) Stability tests of SUPS.

of eight persons in health group, six persons in CHD group, three persons in AF group, and three persons in ASD group were selected and analyzed. All volunteer patients are tested in Beijing Chaoyang Hospital and Beijing Anzhen Hospital, signed informed consent was obtained for each participant according to institutional guidelines before the procedure commenced. A mathematical "remodeling" based on the feature points make the crude pulse waveform curve acquired from SUPS more easy to compare and analyze. The postsignal processing procedures was firstly carried out and shown in Figure S5 in Supporting Information. After that, the feature points (a–g) were determined by characteristic peak analysis. Then the data of pulse signal were carried out normalization processing as follow. Time (t) serve as horizontal axis and amplitude (A) serve as oriental axis. Here

$$tin = Tin - Tbn \tag{1}$$

$$Ain = \frac{Vin}{Vbn} \tag{2}$$

$$\overline{A} = \frac{1}{n}\sum_{k=1}^{n} {}^{Ain} \tag{3}$$

$$\overline{t} = \frac{1}{n}\sum_{k=1}^{n} {}^{tin} \tag{4}$$

where T represents time, i represent a–g, respectively (**Figure 4**a), n is the number of pulse cycles. Ten pulse cycles of each case was analyzed. Second, the pulse contour signals of different groups were remodeled according to the distribution of feature points. The points were distributed in similar region of same group (Figure 4a–d). However, it has obvious differences between health and unhealthy group (Figure 4e). For example, $\overline{td}$ of CHD group smaller than health group, because atherosclerosis caused the velocity of tidal wave increased. And it is more easily combined with pattern recognition and big data, which are the basis for artificial intelligence to apply in intelligent diagnosis of cardiovascular disease in the future.

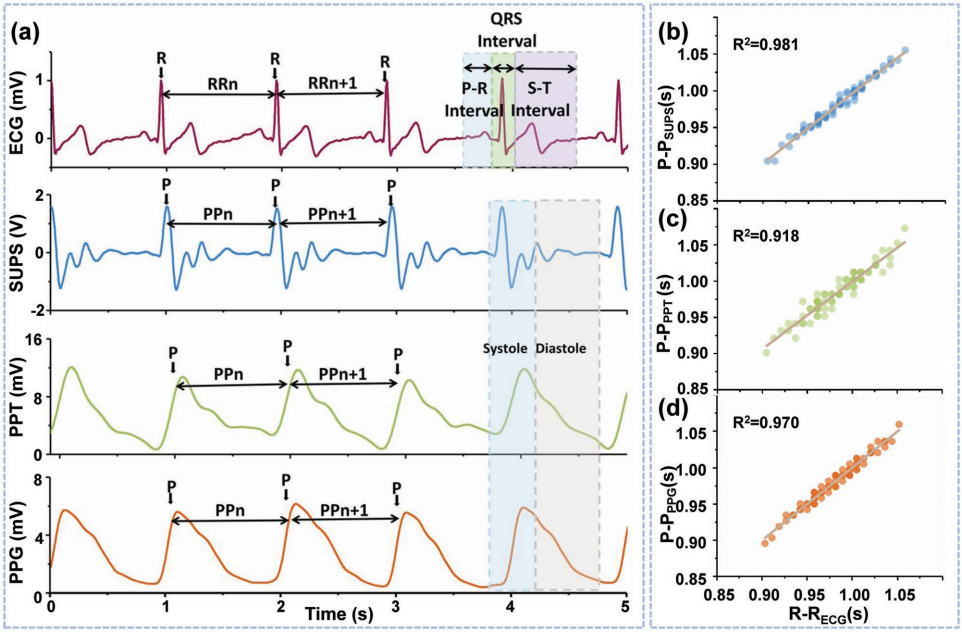

Figure 3. The pulse measurement and the linear fitting analysis of SUPS, PPT, and PPG compared with ECG. a) The comparison of working signals between ECG, SUPS, PPT, and PPG pulse sensors. The linear relationship of b) SUPS, c) PPT, and d) PPG with ECG through the analysis of *R–R* interval.

HRV is the physiological phenomenon of variation in the time interval between heartbeats, it is a powerful predictor of cardiovascular illness and death available.[17] The geometry of HRV Poincare plot has been shown to distinguish between healthy and unhealthy subjects in clinical settings.[18] As shown in Figure 4f–j, the time intervals of P–P_n served as the horizontal

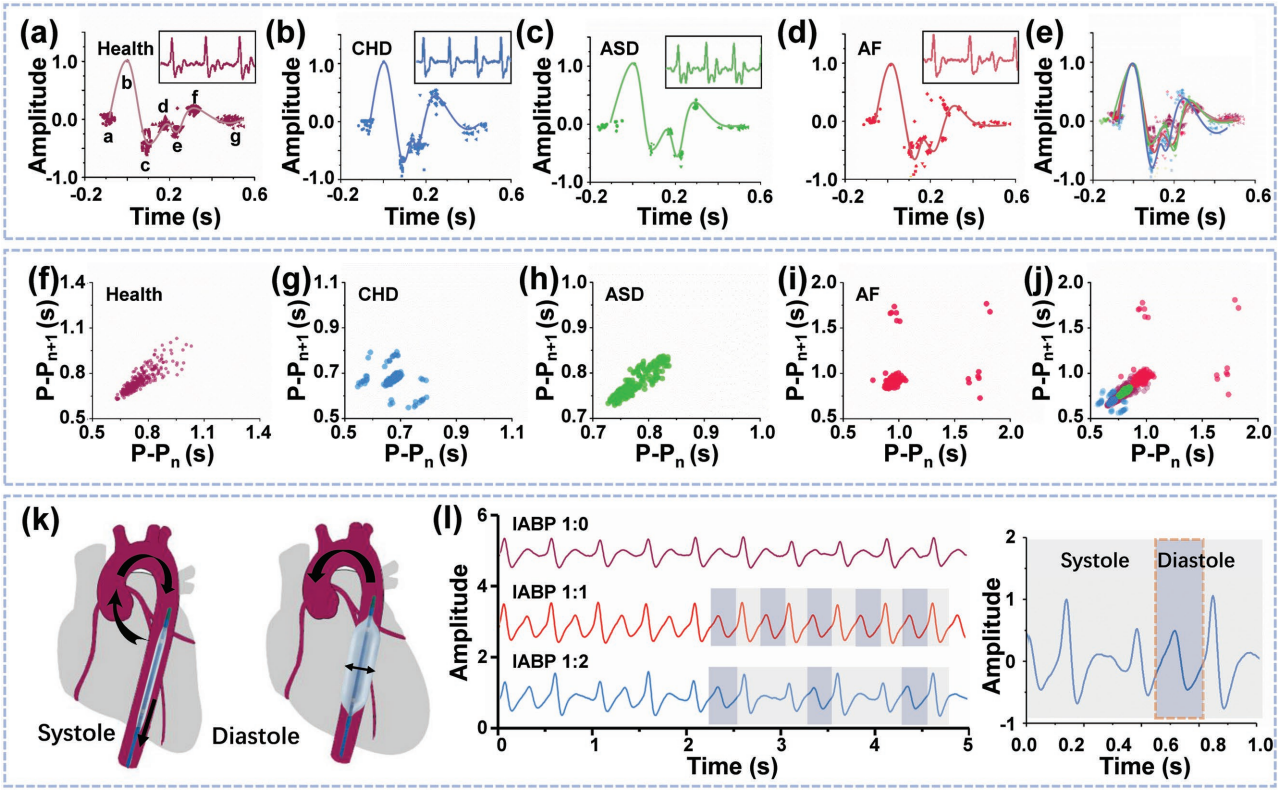

Figure 4. The case analysis results used SUPS. The point distribution and Poincare plot of a,f) Health, b,g) CHD, c,h) ASD, and d,i) AF. The comparison of e) point distribution and j) Poincare plot between health and cardiovascular diseases. k) The systolic and diastolic of heart schematically illustrating the working principle of IABP. l) The radial artery signals of a patient with the various working mode of IABP.

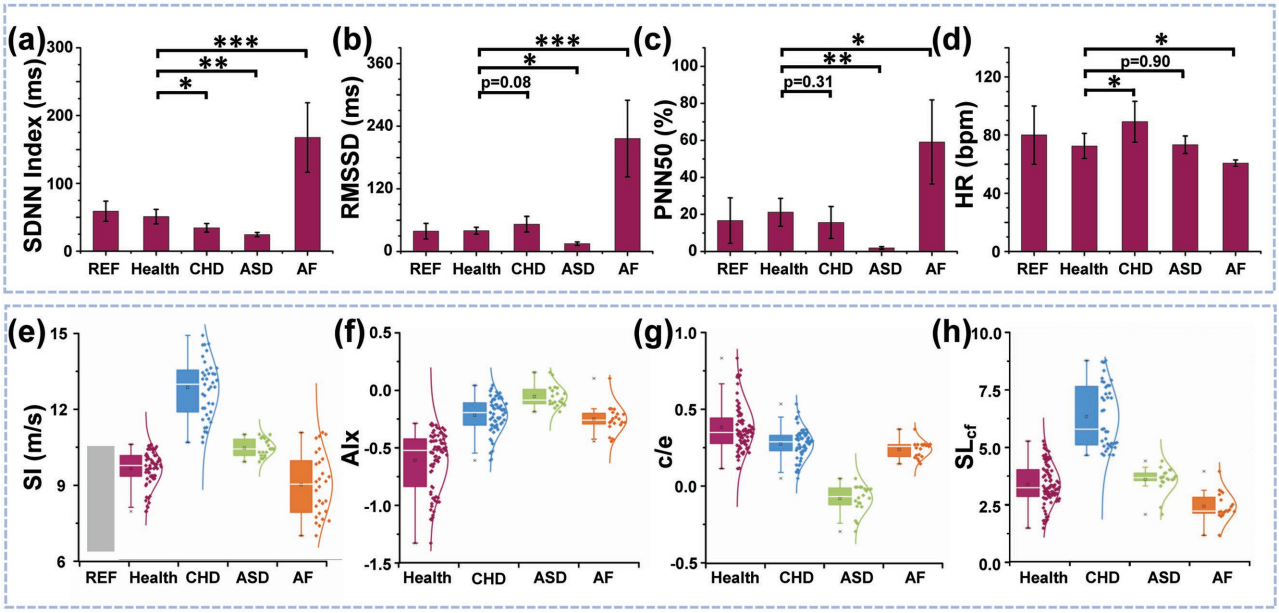

Figure 5. The comparison analysis of heart rate variability, artery stiffness, and LV ejection capacity between health and patients with cardiovascular disease. HRV analysis through time-domain statistical analysis used a) SDNN, b) RMSSD, c) PNN50, and d) HR. Artery stiffness analysis assessed through e) SI, and h) SL_{cf}. Additional load and ejection capacity of LV measured by f) AIx and g) *c*/*e*. All the data (health to AF) are means ± SD; statistics by two-tailed unpaired *t*-test; in HRV analysis $n = 8$ independent cases (health), $n = 6$ independent cases (CHD), and $n = 3$ independent cases (ASD, AF). In pulse contour analysis $n = 80$ pulse cycles (health), $n = 60$ pulse cycles (CHD), and $n = 30$ pulse cycles (ASD, AF), 10 pulse cycles for each cases. *P*-values were calculated by *t*-test. $^{*}P < 0.05$, $^{**}P < 0.01$, $^{***}P < 0.001$ versus control.

axis and $P–P_{n+1}$ served as the vertical axis. The Poincare plot of a healthy sample (Figure 4f) and a patient with CHD (Figure 4g), ASD (Figure 4h), and AF (Figure 4i) were constructed based on radial artery pulse acquired from SUPS. Meanwhile, SUPS achieved the more accurate Poincare plot contribute to the high linearity of *P*–*P* interval and *R*–*R* interval obtain from SUPS and ECG respectively. The geometry of Poincare plot depends on HRV, which regulated by vagal and sympathetic activity.[19,20] From Figure 4f we can see that the healthy subject has a comet or ellipse shaped Poincare plot. However, a patient with CHD has a shorter width and length Poincare plot geometry compared with healthy person as shown in Figure 4g,j. It was reported a longer length before according to the analysis result of ECG,[21] it may be caused by the variation of individual. In addition, an ASD subject has a relative ellipse shape and shorter length (Figure 4h,j) Poincare plot geometry.[20] The geometry of a patient with AF (Figure 4i,j) was irregular, and obvious difference of Poincare plot between health and case samples makes SUPS a useful tool in antidiastole of cardiovascular illness.

Besides, SUPS was tested by a case that implanted intraaortic balloon pump (IABP), whose cardiovascular system was regulated through open and close of the balloon pump. The operation principle of IABP was shown in Figure 4k. The radial artery pulse at various operational modes of IABP (1:0, 1:1, and 1:2) were acquired and compared in Figure 4l. At the working mode of 1:0, IABP did not work and closed. At the working mode of 1:1, when the heart diastole and systole, the balloon pump open (light blue) and close (gray) at the same time as shown in the middle of Figure 4l. At the working mode of 1:2, the heart diastole and systole without balloon pump working at the first respiratory cycle (gray), and then the balloon pump open and close with the heat diastole and systole at the second respiratory cycle (bottom of Figure 4l).[22] SUPS can detect the variation of pulse wave, when the cardiac load or vascular pressure was altered. It is laid the foundation of indicative diagnosis and antidiastole to cardiovascular disease.

Three time-domain HRV indexes defined as SDNN index (mean of the standard deviations of all normal sinus *R*–*R* intervals for all 5 min segments), root-mean-square of successive normal sinus *R*–*R* interval difference (RMSSD), and the percentage of successive normal sinus *R*–*R* intervals >50 ms (PNN50) were calculated from the time series of *R*–*R* intervals based on radial artery pulse acquired from SUPS. As presented in **Figure 5**a–d, the REF (refrence) groups were referred to the reference range of the normal person,[23] and the health groups were referred to the healthy subjects in our samples. Similarly, the SDNN index, RMSSD, and PNN50 of the ASD group were all reduced and have statistical difference ($P < 0.01$, $P < 0.05$, $P < 0.01$), it may cause by the autonomic nervous dysfunction. The SDNN index, RMSSD, and PNN50 of AF group were all increased significantly and have statistical difference ($P \ll 0.01$, $P \ll 0.01$, $P < 0.01$), it relate to the severe arrhythmias. The SDNN index of CHD groups was reduced compared with health group and has statistical difference ($P < 0.05$), PNN50 was reduced but has no statistical difference ($P = 0.31$) and RMSSD was slightly increase, which have a little difference from the previous report,[24] possibly caused by the too little sample size. Furthermore, the heart rate (HR) was also calculated. Through the time-domain analysis of HRV, we can indicate that SUPS was a powerful tool for indicative diagnosed of arrhythmia (atrial fibrillation) by time-domain HRV indexes analysis.

Table 2. Statistical analysis and comparison of SI, AIx, c/e, and SL_{cf} between health, CHD, ASD, and AF. P-values were calculated by t-test. $^{*}P < 0.05$, $^{**}P < 0.01$, $^{***}P < 0.001$ versus control.

	Mean	SD	P	Mean	SD	P	Mean	SD	P	Mean	SD	P
Health	9.49	0.66		–0.61	0.26		0.38	0.16		3.34	0.90	
CHD	12.59	1.19	***	–0.21	0.15	***	0.27	0.10	***	6.35	1.40	***
ASD	10.28	0.33	*	–0.05	0.09	***	–0.09	0.09	***	3.56	0.55	0.159
AF	8.88	1.19	***	–0.25	0.12	***	0.24	0.05	**	2.36	0.60	***

Furthermore, other indexes based on pulse contour analysis were used to distinguish and antidiastole of cardiovascular illness. Therefore, an index of large artery stiffness (SI) was used to assess the clinical applicability of SUPS. SI was obtained from subject height and the time delay between direct and reflected waves in the radial artery pulse[25]

$$\mathrm{SI} = \frac{H}{\Delta T} \tag{5}$$

Here, H is the height of the person, ΔT is time delay between direct wave and reflected wave, $\Delta T = T\mathrm{d} - T\mathrm{b}$. As shown in Figure 5e and **Table 2**, SI of CHD were higher than health, and have statistical difference ($P \ll 0.01$).

Aortic augmentation index (AIx) has been proposed as an index of additional load of left ventricle (LV),[26] and is associated with cardiovascular risk. AIx was defined as the increment in pressure from the first systolic shoulder (inflection point) to the peak pressure of the aortic pressure waveform,[27] which is dependent on the length of respiratory cycle and HR

$$\mathrm{AIx} = \frac{A\mathrm{c} - A\mathrm{d} - A\mathrm{e} - A\mathrm{f}}{A\mathrm{b}} \tag{6}$$

Here, A_i is amplitude, i are refer to the feature points of SUPS a–g, respectively (Figure 4a). Patients with ASD whose blood flow between atria of the heart instead of ventricle, resulted in the change of additional load of LV. Hence, AIx of ASD patients were obtained as shown in Figure 5f and Table 2, it was significantly higher than that of healthy men, and have distinct statistical difference ($P \ll 0.01$). From all above, antidiastole to ASD can be made through the variation of AIx.

Moreover, a more compact index was selected to evaluate the LV ejection capacity, which was c/e

$$c/e = A\mathrm{e} - A\mathrm{c} \tag{7}$$

As shown in Figure 5g and Table 2, the c/e index of ASD was far more below the health group because of the defect of atrial septal, since the low-pressure overload of the right atrium for the patients with ASD.[28] c/e can be a critical substitution index of AIx to antidiastole ASD. Ulteriorly, integrate the analysis result of AIx and c/e, more accurately antidiastole to ASD can be achieved through the pulse wave data acquired from SUPS.

In addition, we provided another parameter to evaluate the arterial stiffness to substitute or combine with SI to antidiastole CHD. As mentioned above, c is the percussion wave, the LV blood ejection was transmitted by the elastic arterial wall, f is the dicrotic wave, a reflective oscillatory wave occurring when the blood injects into the aortic valve by pressure in the aorta. The time parameter of feature point (Ti) can be used in assessment of disease and illness, owing to the high accuracy of feature points in time measured by SUPS. Hence, SL_{cf} was put forward and can be act as an indicator of arterial elasticity

$$\mathrm{SLcf} = \frac{Af - Ac}{Tf - Tc} \tag{8}$$

T_i refers to time. As shown in Figure 5h and Table 2, SL_{cf} of CHD was higher than health group obviously, and has significantly statistical difference ($P \ll 0.01$).

As mentioned above, SUPS have high resolution in time; therefore, it has unique advantage in PWV measurements. PWV was accepted as the robust, simple, and reproducible method to determine the regional arterial stiffness. Hence, PWV was measured by use two sensors at different positions on the radial artery of the wrist simultaneously, two sensors were apart from 4.5 cm. This distance divided by the time interval associated with a definite peak (feature point of b) in the waveform determined PWV of the regional artery. Here, the PWV is different from the commonly used abPWV (ankle-brachial PWV) and cfPWV (carotid\-femoral PWV) in clinical. Due to the high resolution in time, our SUPS is expected to be applied for regional artery PWV measurement, which will be more convenient and accurate. In order to demonstrate the ability of SUPS to perceive changes of PWV, the PWV of a 24 year old man before and after exercise (jogs 500 meters) were measured. The PWV increased from 8.92 ± 1.50 to 10.83 ± 1.77 m s^{-1} where the time separation is 5.04 and 4.15 ms, respectively (**Figure 6**a–c). The changes of PWV value measured by SUPS (21.4%) were comparable with the typical PWV change ($11.6 \pm 8.3\%$) measured by tonometry before and after isometric exercise.[29]

The key features of a wireless pulse sensor system were exploits bluetooth technology to monitor pulse waveform through SUPS. A block diagram of the functional components in wireless pulse sensor system is presented in Figure 6d. A wireless link established by 2.4 GHz RF associated with the sensor system and an external device, such as smartphone, tablet, and PC. This system integrates components of SUPS, analog-digital conversion (ADC, 16-bit), 8M-bit data storage, and bluetooth chip. The ADC digitizes the output of SUPS and the bluetooth chip enables wireless data transmission.

The quality of the pulse signal is significant dependent on the sensor-skin interfaces.[30] The shape and geometry of the human body are typically irregular and complex. The SUPS can be adapted to various human body regions as benefited from its flexibility and ultrasensitivity (including the carotid

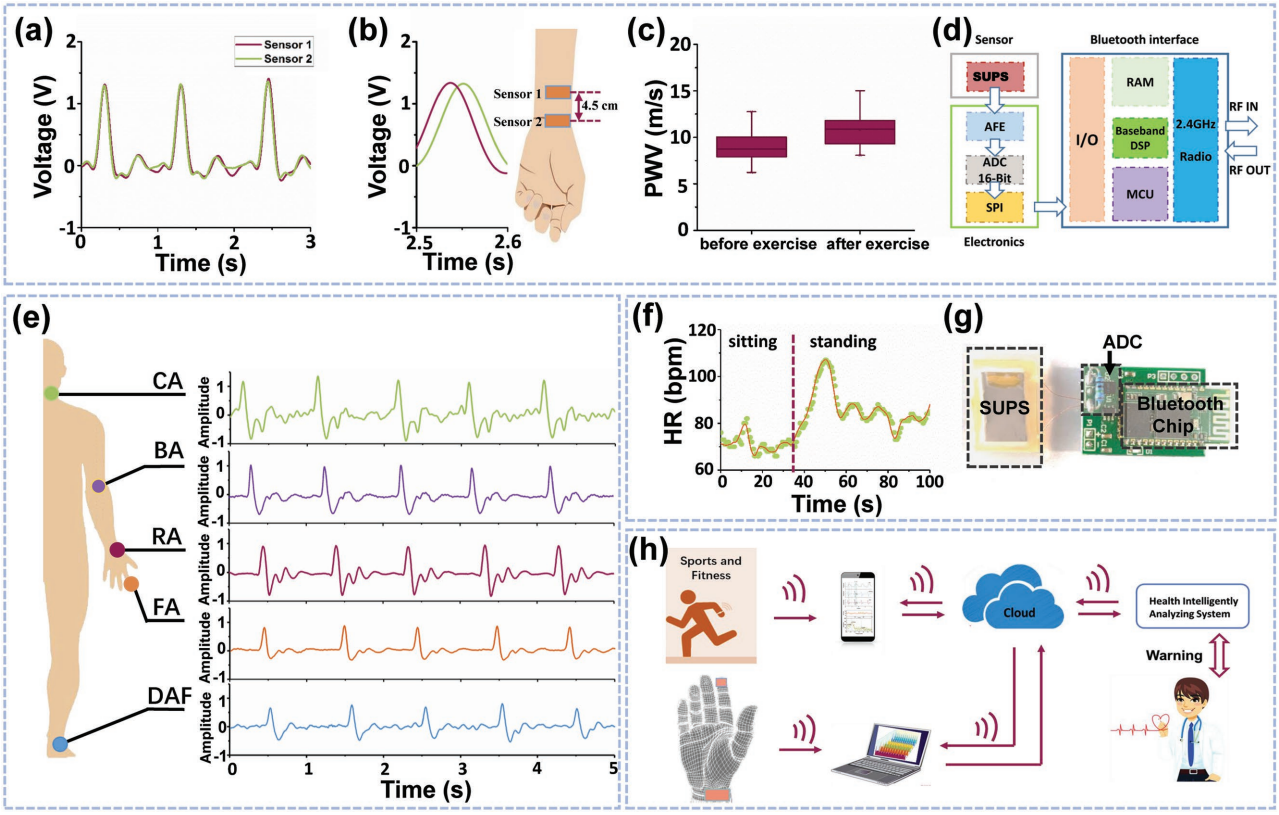

Figure 6. The signal output changes on various artery position and exercise, the components and combination with big data, cloud technology of wireless pulse sensor system. a) The signal output of two SUPS pressed on the radial artery with the distance of 4.5 cm. b,c) The radial artery signal output of SUPS before and after exercise. d) A block diagram of the components in wireless pulse sensor system. e) The signal output of SUPS pressed on various artery position. f) Changes in heart rate during the process of sitting and standing up. g) Image of wireless health monitoring system based on SUPS. h) Illustration of intelligent mobile diagnosis system.

artery, the brachial artery, the radial artery, the finger, and the ankle artery region, and sense various amplitudes of pulses) (Figure 6e). These pulse waveforms have more similar features, which lead to acquire the PWV more easily. SUPS can easily detect changes in heart rate during human activity. For example, when the body is in the process of standing up, the heart rate rises and then falls to a value slightly higher than sitting (Figure 6f). However, the effect of body movement on the waveform of pulse signal is weak, because we can also accurately identify the feature peak position of the pulse signals and calculate the heart rate from the acquired signals (Figure S6c,d and Video S3, Supporting Information).

Based on this, this SUPS is expected to be applied in intelligent mobile diagnosis system. The system including an end-to-end solution that can continuously acquire pulse wave information. Meanwhile, a long-term measurement on the same human subject was carried out as shown in Figures S7 and S8 in Supporting Information. Through the general network and intelligent terminal, we can get expert advice and other feedback for a patient (Figure 6g,h). The system is expected to be applied in on-line monitoring, intelligent mobile diagnosis, and prevention of cardiovascular disease.

In summary, we developed a self-powered ultrasensitive pulse sensor to convert human pulse biomechanical signal into electric signal. The SUPS has self-powered, ultrasensitive, high PSNR, low cost price, and excellent output performance. Additionally, SUPS can directly acquire voltage signal which is consistent with second derivative of conventional pulse signal without complex circuit design, mathematical operations, and the resulting error. It has been demonstrated that the SUPS was possessed of the important value in indicative diagnosis and antidiastole of cardiovascular diseases such as arrhythmia, coronary heart disease, and atrial septal defect. PWV can be measured by simultaneously using two SUPS, which can be used to indicate the degree of arteriosclerosis. We also build a wireless cardiovascular health monitor system based on SUPS, which is expect to be applied in intelligent mobile diagnosis and offer new opportunities in cardiovascular diseases prevention by the long-term monitoring of physiological pulse signal.

Experimental Section

Characterization Methods: The open-circuit voltage was measured by Keithley oscilloscope DPO6450, the short-circuit current, and transferred charge were measured using a Keithley 6517 system electrometer. All scanning electron microscope (SEM) images were taken by Hitachi field emission SEM (SU 8020). All atomic force microscopy (AFM) images were taken by Asylum Research MFP-3D-SA-DV.

Fabrication of the SUPS: The fabricated nanostructured Kapton film and Cu film were processed by inductively coupled plasma (ICP) etching system (SENTECH/SI 500). As Figure S1b in Supporting Information shows, a piece of 100 μm Kapton film was rinsed with menthol, isopropyl alcohol, and deionized water. Then a 10 nm thick Au was sputtered onto the Kapton surface, which acted as the mask for the etching process. Subsequently, this Kapton was etched through the ICP reactive ion etching for 300 s. The reaction gas was 15.0 sccm Ar, 10.0 sccm O_2, and 30.0 sccm CF_4 in the ICP process. The two ICP power were 400 and 100 W, respectively. Finally, the Cu was deposited on nanostructured Kapton surface by magnetron sputter for 900 s and the sputter power was 100 W. The Cu electrode was deposited by magnetron sputter (Denton Discovery 635). Then PDMS (Dow Corning Sylgard 184 Silicone Encapsulant) mixed with specific ratio of curing agent (10:1) was spin-coated on the device as the second package layer after solidifying in 80 °C for an hour,

Statistical Analysis: The *t*-test was used to compare mean values in groups of samples for all experiments. Error bars were calculated using mean ± SD(standard deviation). with a group size $n \geq 3$. All reported *P*-values were calculated for groups with unequal variance using the Origin software program and a two-tailed unpaired *t*-test. Reported *P*-values for all experiments correspond to $^*P < 0.05$, $^{**}P < 0.01$, $^{***}P < 0.001$.

Case Test: The subject was at least 5 min resting and avoided smoking and drinking coffee within 30 min before the survey. The measured person to take the seat, the best sitting back chair, exposed right wrist, elbow placed at the same level with the heart. In studies, all pulse measurements were performed by the wireless health monitoring system based on SUPS, in a quiet room, with comfortable temperature. Every volunteer patient who agreed to participate in this study received detailed explanation before the procedure commenced and talking was avoided during the measurements.

Supporting Information

Supporting Information is available from the Wiley Online Library or from the author.

Acknowledgements

H.O., J.J.T., and G.L.S. contributed equally to this work. The authors thank Dr. H.T. Yuan (BINN of CAS) for assistance in inductively coupled plasma etching system. The authors are also grateful to all the volunteer patients and laboratory members for their cooperation in this study. This work was supported by the National Key R & D project from Minister of Science and Technology, China (2016YFA0202703), NSFC (31571006, 81601629), Beijing Talents Fund (2015000021223ZK21), and "Thousands Talents" program for pioneer researcher and his innovation team. Z.L., Z.L.W., H.O.Y., and J.J.T. conceived the project. H.O.Y., J.J.T., B.J.S., and Z.L. carried out the SUPS fabrication and electrical characteristic work. H. L., H.O.Y., and L.M.Z. accomplish the material characterization. H.O.Y. designed the PCBA (Printed Circuit Board Assembly) of wireless pulse sensor system. G.L.S., J.J.T., and H.O.Y. designed and carried out the case test. H.O.Y., Y.F.F., G.L.S., J.J.T., and Y.Z. processed the data and carried out the statistical analysis of the pulse signal. All authors discussed and co-wrote the paper. The authors declare that they have no competing interests. All data needed to evaluate the conclusions in the paper are present in the paper and/or the Supporting Information. Additional data related to this paper may be requested from the authors.

Conflict of Interest

The authors declare no conflict of interest.

Keywords

cardiovascular diseases, pulse sensors, self-powered system, triboelectric nanogenerators

Received: June 20, 2017
Revised: July 27, 2017
Published online:

[1] I. Abubakar, T. Tllmann, A. Banerjee., *Lancet*, **2015**, *385*, 117.
[2] H. C. McGill, C. A. McMahan, S. S. Gidding, *Circulation* **2008**, *117*, 1216.
[3] a) J. Rivnay, P. Leleux, M. Ferro, M. Sessolo, A. Williamson, D. A. Koutsouras, D. Khodagholy, M. Ramuz, X. Strakosas, R. M. Owens, *Sci. Adv.* **2015**, *1*, e1400251; b) P. Leleux, J. Rivnay, T. Lonjaret, J. M. Badier, C. Bénar, T. Hervé, P. Chauvel, G. G. Malliaras, *Adv. Healthcare Mater.* **2015**, *4*, 142.
[4] a) A. Campana, T. Cramer, D. T. Simon, M. Berggren, F. Biscarini, *Adv. Mater.* **2014**, *26*, 3874; b) H. Fang, K. J. Yu, C. Gloschat, Z. Yang, E. Song, C.-H. Chiang, J. Zhao, S. M. Won, S. Xu, M. Trumpis, *Nat. Biomed. Eng.* **2017**, *1*, 0055.
[5] Y. Liu, J. J. Norton, R. Qazi, Z. Zou, K. R. Ammann, H. Liu, L. Yan, P. L. Tran, K.-I. Jang, J. W. Lee, *Sci. Adv.* **2016**, *2*, e1601185.
[6] a) T. J. Niiranen, J. Mäki, P. Puukka, H. Karanko, A. M. Jula, *Hypertension* **2014**, *64*, 281; b) C. M. Villalva, X. L. M. Lopez-Alvarez, M. M. Rodriguez, M. J. M. Freire, O. Q. Veloso, L. C. Guede, S. V. Dosantos, M. B. Ramos, *AIMS Med. Sci.* **2017**, *4*, 164.
[7] S. Gong, W. Schwalb, Y. Wang, Y. Chen, Y. Tang, J. Si, B. Shirinzadeh, W. Cheng, *Nat. Commun.* **2014**, *5*, 3132.
[8] M. Elgendi, *Curr. Cardiol. Rev.* **2012**, *8*, 14.
[9] T. Tamura, Y. Maeda, M. Sekine, M. Yoshida, *Electronics* **2014**, *3*, 282.
[10] a) F.-R. Fan, Z.-Q. Tian, Z. L. Wang, *Nano Energy* **2012**, *1*, 328; b) S. Niu, X. Wang, F. Yi, Y. S. Zhou, Z. L. Wang, *Nat. Commun.* **2015**, *6*, 8975; c) J. Wang, S. Li, F. Yi, Y. Zi, J. Lin, X. Wang, Y. Xu, Z. L. Wang, *Nat. Commun.* **2016**, *7*, 12744.
[11] a) Q. Zheng, B. J. Shi, F. R. Fan, X. X. Wang, L. Yan, W. W. Yuan, S. H. Wang, H. Liu, Z. Li, Z. L. Wang, *Adv. Mater.* **2014**, *26*, 5851; b) Q. Zheng, Y. Zou, Y. Zhang, Z. Liu, B. Shi, X. Wang, Y. Jin, H. Ouyang, Z. Li, Z. L. Wang, *Sci. Adv.* **2016**, *2*, e1501478; c) W. Tang, J. Tian, Q. Zheng, L. Yan, J. Wang, Z. Li, Z. L. Wang, *ACS Nano* **2015**, *9*, 7867.
[12] a) Y. Ma, Q. Zheng, Y. Liu, B. Shi, X. Xue, W. Ji, Z. Liu, Y. Jin, Y. Zou, Z. An, *Nano Lett.* **2016**, *16*, 6042; b) Q. Zheng, H. Zhang, B. Shi, X. Xue, Z. Liu, Y. Jin, Y. Ma, Y. Zou, X. Wang, Z. An, W. Tang, W. Zhang, F. Yang, Y. Liu, X. Lang, Z. Xu, Z. Li, Z. L. Wang, *ACS Nano* **2016**, *10*, 6510; c) J. Yang, J. Chen, Y. Su, Q. Jing, Z. Li, F. Yi, X. Wen, Z. Wang, Z. L. Wang, *Adv. Mater.* **2015**, *27*, 1316.
[13] a) T. Yamakoshi, J. Lee, K. Matsumura, Y. Yamakoshi, P. Rolfe, D. Kiyohara, K.-i. Yamakoshi, *Plos One* **2015**, *10*, e0143506; b) E. S. Winokur, T. O'Dwyer, C. G. Sodini, *IEEE Trans. Biomed. Circ. Syst.* **2015**, *9*, 581.
[14] Q. Zheng, Y. Jin, Z. Liu, H. Ouyang, H. Li, B. Shi, W. Jiang, H. Zhang, Z. Li, Z. L. Wang, *ACS Appl. Mater. Interfaces* **2016**, *8*, 26697.
[15] A. Burkart, K. Lunau, C. Schlindwein, *J. Pollinat. Ecol.* **2011**, *6*, 118.
[16] E. Von Wowern, G. Ostling, P. Nilsson, P. Olofsson, *Plos One* **2015**, *10*, e0135659.
[17] a) R. Ranpuria, M. Hall, C. T. Chan, M. Unruh, *Nephrol., Dial., Transplant.* **2008**, *23*, 444; b) R. G. Stout, A. Ghobashy, E. Ferneini, P. Wagner, C. Ehrenwerth, S. Qadir, D. G. Silverman, *Anesth. Analg.* **1998**, *86*, U79; c) H. Tsuji, M. G. Larson, F. J. Venditti, E. S. Manders, J. C. Evans, C. L. Feldman, D. Levy, *Circulation* **1996**, *94*, 2850.

[18] a) X. Copie, J. Y. LeHeuzey, M. C. Iliou, R. Khouri, T. Lavergne, F. Pousset, L. Guize, *Pace* **1996**, *19*, 342; b) M. Brennan, M. Palaniswami, P. Kamen, *IEEE Trans. Biomed. Eng.* **2001**, *48*, 1342.
[19] R. E. Kleiger, J. P. Miller, J. T. Bigger, A. J. Moss, *Am. J. Cardiol.* **1987**, *59*, 256.
[20] K. E. J. Airaksinen, M. J. Ikaheimo, M. K. Linnaluoto, M. Niemela, J. T. Takkunen, *Br. Heart J.* **1987**, *58*, 592.
[21] a) R. K. G. Moore, N. Newall, D. Groves, P. Barlow, R. H. Stables, M. Jackson, D. R. Ramsdale, *Int. J. Cardiol.* **2007**, *118*, 4; b) J. Hayano, Y. Sakakibara, M. Yamada, N. Ohte, T. Fujinami, K. Yokoyama, Y. Watanabe, K. Takata, *Circulation* **1990**, *81*, 1217.
[22] J. D. Dedhia, K. R. N. Chakravarthy, A. B. Ahmed, *Indian J. Anaesth.* **2008**, *52*, 387.
[23] A. Wykretowicz, K. Adamska, T. Krauze, P. Guzik, A. Szczepanik, A. Rutkowska, H. Wysoki, *Free Radical Res.* **2007**, *41*, 645.
[24] F. C. Pivatelli, M. A. D. Santos, G. B. Fernandes, M. Gatti, L. C. De Abreu, V. E. Valenti, L. C. M. Vanderlei, C. Ferreira, F. Adami, T. D. De Carvalho, *Int. Arch. Med.* **2012**, *5*, 31.
[25] S. C. Millasseau, R. P. Kelly, J. M. Ritter, P. J. Chowienczyk, *Clin. Sci.* **2002**, *103*, 371.
[26] a) I. B. Wilkinson, J. R. Cockcroft, D. J. Webb, *J. Cardiovasc. Pharmacol.* **1998**, *32*, S33; b) M. F. O'Rourke, G. Mancia, *J. Hypertens.* **1999**, *17*, 1.
[27] R. P. Kelly, S. C. Millasseau, J. M. Ritter, P. J. Chowienczyk, *Hypertension* **2001**, *37*, 1429.
[28] T. Hata, S. Mano, M. Kusuki, H. Matsuura, M. Miyata, T. Yamazaki, S. Nagaoka, *Pace* **2007**, *30*, S212.
[29] C. Reid, *Am. J. Hypertens.* **2004**, *17*, S135.
[30] a) C. Dagdeviren, Y. Su, P. Joe, R. Yona, Y. Liu, Y. Kim, Y. Huang, A. R. Damadoran, J. Xia, L. W. Martin, *Nat. Commun.* **2014**, *5*, 4496; b) M. K. Choi, O. K. Park, C. Choi, S. Qiao, R. Ghaffari, J. Kim, D. J. Lee, M. Kim, W. Hyun, S. J. Kim, *Adv. Healthcare Mater.* **2016**, *5*, 80; c) C. Pang, J. H. Koo, A. Nguyen, J. M. Caves, M. G. Kim, A. Chortos, K. Kim, P. J. Wang, J. B. H. Tok, Z. Bao, *Adv. Mater.* **2015**, *27*, 634.

